Stabilizing Bound O_2 in Myoglobin by Valine[68] (E11) to Asparagine Substitution[†,‡]

Szymon Krzywda,[||,§] Garib N. Murshudov,[||,⊥] Andrzej M. Brzozowski,[||] Mariusz Jaskolski,[§] Emily E. Scott,[▽] Sarah A. Klizas,[▽] Quentin H. Gibson,[▽] John S. Olson,[▽] and Anthony J. Wilkinson*[,||]

Department of Chemistry, University of York, York YO1 5DD, U.K., Institute of Bioorganic Chemistry, Polish Academy of Sciences, and Department of Crystallography, Adam Mickiewicz University, Poznan, Poland, CLRC Daresbury Laboratory, Daresbury, Warrington WA4 4AD, U.K., and Department of Biochemistry and Cell Biology and the W. M. Keck Center for Computational Biology, Rice University, Houston, Texas 77005-1892

Received May 27, 1998; Revised Manuscript Received August 27, 1998

ABSTRACT: The isopropyl side chain of valine[68] in myoglobin has been replaced by the acetamide side chain of asparagine in an attempt to engineer higher oxygen affinity. The asparagine replacement introduces a second hydrogen bond donor group into the distal heme pocket which could further stabilize bound oxygen. The Val[68] to Asn substitution leads to ∼3-fold increases in oxygen affinity and 4−6-fold decreases in CO affinity. As a result, the *M*-value (K_{CO}/K_{O_2}) is lowered 15−20-fold to a value close to unity. An even larger enhancement of O_2 affinity is seen when asparagine[68] is inserted into H64L sperm whale myoglobin which lacks a distal histidine. The overall rate constants for oxygen and carbon monoxide binding to the single V68N myoglobin mutants are uniformly lower than those for the wild-type protein. In contrast, the overall rate constant for NO association is unchanged. Analyses of time courses monitoring the geminate recombination of ligands following nanosecond and picosecond flash photolysis of MbNO and MbO_2 indicate that the barrier to ligand binding from within the heme pocket has been raised with little effect on the barrier to diffusion of the ligand into the pocket from the solvent. The crystal structures of the aquomet, deoxy, oxy, and carbon monoxy forms of the V68N mutant have been determined to resolutions ranging from 1.75 to 2.2 Å at 150 K. The overall structures are very similar to those of the wild-type protein with the principal alterations taking place within and around the distal heme pocket. In all four structures the asparagine[68] side chain lies almost parallel to the plane of the heme with its amide group directed toward the back of the distal heme pocket. The coordinated water molecule in the aquomet form and the bound oxygen in the oxy form can form hydrogen-bonding interactions with both the Asn[68] amide group and the imidazole side chain of His[64]. Surprisingly, in the carbon monoxy form of the V68N mutant, the histidine[64] side chain has swung completely out the distal pocket, its place being taken by two ordered water molecules. Overall, these functional and structural results show that the asparagine[68] side chain (i) forms a strong hydrogen bond with bound oxygen through its $-NH_2$ group but (ii) sterically hinders the approach of ligands to the iron from within the distal heme pocket.

The capacity of the polypeptide chains of myoglobin and hemoglobin to adapt the properties of their heme cofactors to discriminate effectively between O_2 and CO ligands is essential for aerobic respiration. A large number of studies have addressed the structural basis of this discrimination, the most recent of which have used site-directed mutagenesis approaches (*1*, *2*). These experiments have evaluated quantitatively the contribution of the distal histidine residue (E7) and shown that the polarity of its imidazole side chain is dominant in governing the relative affinities for CO and O_2 as manifested in the *M*-value ($M = K_{CO}/K_{O_2}$). In deoxymyoglobin, the N_ϵ-H of the imidazole stabilizes a noncovalently bound water molecule in the distal pocket through the formation of a hydrogen bond. This water molecule has to be displaced from the distal pocket before diatomic ligands can approach the iron. For O_2 binding, the unfavorable free energy associated with the loss of the water−imidazole hydrogen bond is offset by the formation of a stronger hydrogen bond between the imidazole species and the highly polar iron−dioxygen complex. In contrast, the Fe−C═O complex is much less polar, and the ligand−imidazole interaction does not compensate for the requirement to displace H_2O from deoxyMb.[1] As a result, O_2 and CO affinities in myoglobin are 100-fold higher and 5−10-fold lower, respectively, than in model heme compounds (*1*, *3*).

[†] Supported by Grant GR/E 98867 from the Science and Engineering Research Council, U.K. (A.J.W.), and by United States Public Health Service Grants GM-35649 (J.S.O.), GM14276 (Q.H.G.), and HL-47020 (J.S.O.), Grant C-612 (J.S.O.) from the Robert A. Welch Foundation, and the W. M. Keck Foundation. S.K. was supported by British Council Travel Grant WAR/922/015. G.N.M. was supported by a BBSRC grant awarded to CCP4. M.J. was supported by a grant from the Howard Hughes Medical Institute. E.E.S. was supported by a traineeship from the United States Public Health Service Training Grant GM08280.

[‡] Brookhaven Protein Data Bank codes: 1mwd, wild-type deoxyMb; 1mwc, wild-type MbCO; 1mdn, V68N deoxyMb; 1m6c, V68N MbCO; 1mno, V68N MbO_2; 1m6m, V68N metMb.

[||] University of York.

[§] Polish Academy of Sciences & Adam Mickiewicz University.

[⊥] CLRC Daresbury Laboratory.

[▽] Rice University.

[1] Abbreviations: Mb, myoglobin; MbCO, carbon monoxymyoglobin; MbO_2, oxymyoglobin; deoxyMb, deoxymyoglobin; ns, nanosecond; ps, picosecond.

10.1021/bi9812470 CCC: $15.00
Published on Web 10/22/1998

These observations suggested that the introduction of a second hydrogen bond donor group adjacent to the bound ligand, through a valine[68] (E11) to threonine mutation, might enhance ligand discrimination even further. Characterization of this mutant showed that although the substitution does lower CO affinity 6-fold, the predominant effect is a 17-fold decrease, not increase, in K_{O_2} (*4*). The crystal structure of the V68T protein reveals that the −OH group of threonine[68] donates a hydrogen bond to the main chain carbonyl oxygen on histidine[64] with the result that the nonbonding electrons of the hydroxyl oxygen are oriented toward the iron. This orientation stabilizes noncovalently bound water in deoxymyoglobin but destabilizes bound O_2 which has a partial negative charge (*5*).

Unexpectedly, the replacement of leucine[29] (B10) with phenylalanine lowers the *M*-value of myoglobin by a factor of 10 by markedly raising the affinity for O_2 and leaving that for CO unchanged. This effect was interpreted in terms of favorable electrostatic interactions between the positive edge of the phenyl multipole and the partial negative charge on the second bound oxygen (*6*). Goldberg and co-workers have shown that the abnormally high oxygen affinity of *Ascaris* hemoglobin is due to an additional hydrogen bond between bound O_2 and a Tyr at the B10 position (*7*). The single L29Y (B10) mutation in sperm whale myoglobin fails to mimic this behavior (*8*), although K_{O_2} is increased by the triple substitution H64Q-L29Y-T67R (*9*).

To examine the role of polar interactions in the distal pocket further, we have replaced valine[68] with asparagine in a second effort to provide a hydrogen-bonding interaction from the E11 position. The side chain of asparagine[68] is roughly the same size as that of leucine, whose introduction at position 68 has minimal effects on the structure and function of myoglobin (*10*). The asparagine amide group has the capacity to serve as either a hydrogen bond donor or a hydrogen bond acceptor. Infrared spectroscopy data of Boxer and co-workers have shown that the asparagine[68] mutation lowers the wavenumber of νCO from ∼1945 to 1915 cm^{-1} in human myoglobin (*11*). This decrease indicates that the asparagine side chain is oriented with its $-NH_2$ group toward the bound CO, providing an additional positive electrostatic field adjacent to the bound ligand which decreases the C═O bond order (*12*). Such an orientation is expected to favor oxygen binding by providing an additional hydrogen bond to the highly polar Fe−O_2 complex. To test these interpretations, we have determined the high-resolution crystal structures of the aquomet, oxy, CO, and deoxy forms of the V68N mutant. In addition, the O_2, CO, and NO binding properties of V68N mutants of both pig and sperm whale Mb have been characterized in detail.

The V68N mutants of pig and sperm whale myoglobins have been examined in previous studies of folding and stability in myoglobin (*13*, *14*). Heme loss is faster from this mutant; however the most dramatic effects are on the stability of the apoprotein which exists as a molten globule even in the absence of protein denaturants. Two naturally occurring variants of hemoglobin, Hb-Bristol (βE11 Asp) and Hb-Milwaukee-I (βE11 Glu), have polar substitutions at E11 which decrease stability and increase autoxidation (*15*). Lehmann assumed that the instability is due to the polarity of the acid group and not to a markedly altered tertiary structure of the mutant protein. His interpretation is confirmed by the high-resolution structures determined in this work.

EXPERIMENTAL PROCEDURES

Preparation of Mutants. The valine[68] to asparagine substitution was introduced by oligonucleotide-directed mutagenesis of the pig myoglobin coding sequence. Wild-type and mutant myoglobins were expressed from the λ P_L promoter as fusion proteins with the N-terminal 31 residues of bacteriophage λ CII connected via a tetrapeptide (I-E-K-R) which serves as a protease cleavage site (*16*, *17*). Overproduction is induced by raising the growth temperature of the cryptic λ lysogen *Escherichia coli* M5219, which harbors the temperature-sensitive cI^{857} mutation, to the nonpermissive temperature (from 28 to 42 °C). The fusion protein is expressed as inclusion bodies from which intact myoglobin can be generated following resuspension in urea, reconstitution with hemin, and mild trypsin treatment (*18*). This expression strategy allows V68N myoglobin to be purified in high yield, avoiding the problems associated with the intracellular instability of V68N apomyoglobin, which were encountered when sperm whale V68N was expressed constitutively (*13*). The sperm whale V68N and H64L/V68N myoglobins were constructed by cassette mutagenesis, expressed in *E. coli* TB1 cells, and purified as described in Springer et al. (*3*) and Hargrove et al. (*13*).

Preparation of Crystals. Crystals of wild-type and mutant metMbs were grown in hanging drops from 72−80% (v/v) stock solutions of saturated ammonium sulfate in 0.1 M phosphate buffer (pH 7.1) and 10 mg/mL protein. For the aquomet form, crystals were transferred to a solution of mother liquor containing 25% sucrose and 10% glucose. After a 30-min soak in this cryoprotectant solution, a crystal was rapidly frozen in a stream of liquid nitrogen gas at 150 K. Freezing of crystals in this way extended their lifetime in the X-ray beam and extended the resolution to which data could be collected (Table 1). To establish that crystal freezing is not accompanied by significant alteration in the protein structure, a room-temperature data set was collected from a V68N myoglobin crystal, mounted in a quartz capillary in the usual manner.

For the preparation of crystals of the ferrous forms, the metMb crystals were transferred initially to a round-bottomed flask containing a 5-mL solution of an 80% (v/v) saturated stock solution of ammonium sulfate in 100 mM phosphate buffer (pH 7.1), 10% glucose, 10% sucrose (solution A) that had been previously bubbled with argon gas. Argon was passed through the solution for a further 1 h; 40 mg of sodium dithionite was added dropwise to the solution over a period of 30 min. The crystals changed color noticeably after a few minutes. These deoxymyoglobin crystals were then transferred to a deoxygenated cryoprotectant solution and flash-frozen as before.

For the preparation of CO-myoglobins, the same procedure was followed except that CO gas was bubbled slowly over a period of 45 min through the suspension of the freshly reduced crystals. The sealed flask was then left to stand for a period of 2−16 h. The crystals were then transferred to a solution of deoxygenated and CO-equilibrated cryoprotectant solution and flash-frozen.

Oxymyoglobin crystals were prepared as follows. Deoxymyoglobin crystals prepared as described above were washed

Table 1: Data Collection, Processing, and Refinement Statistics

						Met-Asn[68]	
	deoxy-Wt	CO-Wt	deoxy-Asn[68]	CO-Asn[68]	oxy-Asn[68]	150 K	293 K
I21 unit cell							
a (Å)	122.1	122.2	122.0	122.1	122.2	122.3	124.2
b (Å)	42.1	42.2	42.2	42.3	42.1	41.9	42.6
c (Å)	91.5	91.7	91.5	91.6	91.6	91.5	92.3
β (deg)	92.9	92.6	92.7	92.5	92.6	92.6	92.7
completeness (%)	96.5	98.0	96.7	94.7	96.7	98.7	96.8
resolution (Å)	1.80	1.70	1.98	1.90	1.95	1.80	2.27
R_{merge}[a] (%)							
overall	4.0	3.8	6.8	4.2	4.8	5.4	6.6
highest resolution	29.1	24.9	22.0	21.4	23.7	38.4	22.7
mean $I/(\sigma I)$	21.4	23.4	19.5	22.8	22.3	16.5	15.7
unique reflections	42068	48082	32221	35786	34441	42945	21875
observations per reflection	7.9	6.1	8.5	5.8	5.4	10.0	5.6
no. of atoms							
total	3016	3097	3007	3050	3024	3046	2676
solvent	456	522	444	486	440	493	195
R_{cryst}[b]	19.6	18.9	19.8	19.2	19.1	21.2	17.8
no. of reflections	38972	45654	29512	33640	30873	40678	20626
free R_{cryst}	24.3	23.7	26.2	26.1	25.1	26.5	25.5
no. of reflections	2047	2425	1560	1788	1637	2163	1092
rms_{bond} (Å)	0.013	0.020	0.014	0.019	0.015	0.015	0.016
rms_{angle} (deg)	0.030	0.035	0.033	0.037	0.034	0.034	0.051
rms_{planes} (Å×e2 1−4 distance)	0.031	0.043	0.037	0.042	0.036	0.035	0.058
average *B*-value (Å^2)							
main chain	24.8	23.5	28.2	26.0	25.7	29.6	29.1
side chain	29.9	28.5	32.8	31.6	31.0	33.7	33.3
solvent	47.1	45.3	50.0	46.8	48.0	49.7	56.9

[a] $R_{merge} = \sum|I_i - I_n|/\sum|I_n|$, where I_i is an intensity *hkl* and I_n is the average of the observed equivalents. [b] $R_{cryst} = \sum_{hkl}||F_{obs}| - |F_{calc}||/\sum_{hkl}|F_{obs}|$, where $|F_{obs}|$ and $|F_{calc}|$ are magnitudes of the observed and calculated structure factor amplitudes of a reflection *hkl*, respectively.

in solution A to remove excess dithionite and its reaction products. A crystal was then exposed to air for 10−15 min before being transferred to cryoprotectant solution and flash-frozen.

Data Collection and Refinement. All data sets were collected on an R-axis II image plate detector mounted on a Rigaku rotating copper anode X-ray source (λ = 1.54 Å). The data were processed using DENZO and scaled using the CCP4 suite of programs (*19*, *20*; Table 1).

The starting model for refinement of the V68N aquomet-Mb room-temperature structure was the coordinate set for wild-type pig aquometMb (1myg.pdb). The structure was refined in steps of rigid body refinement followed by cycles of atomic positional and temperature factor refinement using REFMAC and manual model building using the X-AUTOFIT and X-SOLVATE routines implemented in the molecular graphics program QUANTA (*21*, *22*).

Refinement of the low-temperature crystal structures proved to be more complex with refinement stalling when the R_{cryst} fell to ∼23%. This problem was overcome through the introduction and refinement of an overall anisotropic temperature factor parameter to take account of lattice perturbations introduced during the process of freezing the crystals. The first structure to be refined in this way was the azido form of wild-type myoglobin which was solved to 1.75-Å resolution (*23*). These MbN_3 coordinates, with the azide ligands, asparagine[68] side chains, and solvent molecules deleted, formed the starting model for refinement of all of the low-temperature structures described here. Refinement was carried out using the program REFMAC as described above, except that an overall anisotropic *B*-value was refined (*23*). Electron density maps calculated with coefficients $2mF_{obs} - dF_{calc}$ (or $mF_{obs} - dF_{calc}$) and α_{calc} were displayed and used to guide manual adjustment of the models, at regular intervals in the course of refinement. Generally, few adjustments were required aside from reconstruction of the mutated position 68 side chains, the addition of ligand atoms, and the addition/deletion of solvent atoms, as appropriate.

Kinetic Measurements. Overall rate constants for O_2, CO, and NO binding to myoglobin were measured in 0.1 M potassium phosphate buffer (pH 7.0), 1 mM EDTA at 20 °C, following the procedures described by Rohlfs et al. (*24*) and Carver et al. (*25*). The kinetics of oxygen binding to pig myoglobin were measured at five different O_2 concentrations (i.e., in solutions equilibrated with gas phases containing 5%, 10%, 20%, 50%, and 100% O_2). NO complexes of Mbs were prepared by passing the proteins through an anaerobic Sephadex G-25 column and then mixing the effluent with an equal volume of buffer that had been preequilibrated with 1 atm of NO gas (final [NO] = 1 mM). The bimolecular rate of NO binding was measured by flash photolysis using a 300-ns dye-laser system.

Detailed procedures for the nanosecond geminate recombination experiments have been described by Carver et al. (*25*) and Gibson et al. (*26*). Photolysis was initiated by either a 30-ps or a 9-ns laser excitation pulse at 532 nm, and absorbance changes were followed at 436 nm.

RESULTS

Crystal Structures of Asn[68] Mb. The V68N mutation involves the substitution of the isopropyl side chain of valine by the acetamide side chain of asparagine, a replacement which is expected to alter both the polarity and the stereochemistry of the distal heme pocket in myoglobin. The crystal structure of V68N aquometMb shows very few

differences from the structure of wild-type pig aquometmyoglobin (*27*). A least-squares superposition of the well-defined main chain atoms of the A and B molecules in the asymmetric unit of the mutant myoglobin with the corresponding atoms in the molecules of the wild-type myoglobin reveals root-mean-squared displacements of 0.3 Å in each case. Least-squares superposition of the A and B molecules in the V68N crystal structure produces a root-mean-squared deviation of 0.2 Å in the positions of the main chain atoms. Differences of this magnitude are typical of those observed among a larger number of crystal structures of different mutants in various ligation states, and we conclude there are no significant overall changes in tertiary structure accompanying the valine to asparagine substitution. Similarly, the effects of crystal freezing appear to be negligible with rms deviations in main chain atoms of 0.27 and 0.30 Å following superposition of the main chain atoms of molecules A and B, respectively, from the coordinates refined against data collected at room temperature and 150 K.

Electron density associated with the environment of the heme group in molecule A of the asymmetric unit is shown in Figure 1 together with a least-squares overlap of the A molecules of the mutant and wild-type structures in this region. The orientation of the asparagine side chain is well-defined with its amide group directed toward the back of the distal pocket. This orientation is similar to that of the side chain of leucine[68] in the crystal structure of the V68L mutant of sperm whale myoglobin (*10*). The plane of the amide moiety is nearly parallel to that of the heme group. Electron density maps calculated with X-ray data extending to 1.8-Å spacing do not allow the oxygen and nitrogen atoms of the amide group to be distinguished. In the V68N aquometMb model, we have arbitrarily positioned the nitrogen of the amide group closer to the iron. This amide nitrogen is situated within weak hydrogen-bonding distance (3.1 Å) of the coordinated water molecule. The latter is also within hydrogen-bonding distance (2.5 Å) of the N_ϵ of histidine[64].

V68N MbO_2. The electron density associated with the oxy form of the V68N protein is shown in the region of the heme pocket of molecule B along with the refined structural model in Figure 2. The shape of the electron density on the distal side of the iron is consistent with the presence of bound oxygen; however, the height of the electron density peak and the high temperature factors for the oxygen atoms relative to those of surrounding atoms imply less than full occupancy (Table 2). The Fe−O−O angle refines to a mean value of 133° in the two molecules of the asymmetric unit (Table 2). The mean ϕ angle, defined as the angle between the plane containing the iron and the two ligand oxygen atoms and the plane formed by the iron, the first oxygen atom, and the pyrrole nitrogen atom NA, is 166°. The second of the bound oxygen atoms appears to form two hydrogen bonds: the first to the His[64] N_ϵ-H and the second to the Asn[68] NH_2 (Table 2). The iron is situated close to the least-squares plane of the pyrrole nitrogens but displaced to the proximal side; the Fe−$N_{pyrrole}$ planar distance is 0.13 Å in both molecules. This again indicates that the crystals are not fully oxygenated and that significant amounts of deoxyMb are present.

Carbon Monoxy Forms of V68N and Wild-Type Pig Myoglobin. The crystal structure of wild-type pig MbCO is very similar to that of sperm whale MbCO in the P6 crystal form (Figure 3A) (*28*). The iron lies in the plane of the pyrrole nitrogens and the Fe−C−O angle refines to a mean value of 157° in the two molecules of the asymmetric unit. The side chains of His (E7) and Val (E11) are in close proximity to the C and O atoms of the ligand (Table 2).

In contrast to MbO_2, extensive changes in the distal heme pocket of pig MbCO are introduced as a consequence of the V68N mutation (Figure 3B; Table 2). These changes were obvious in the first calculated $2mF_o - dF_c$ and $mF_o - dF_c$ maps. The distal histidine side chain has swung out of the pocket away from the CO ligand and toward the solvent. In this 'up' conformation, the imidazole side chain makes what appear to be strong hydrogen-bonding/electrostatic interactions with the heme 6-propionate carboxylate group, the main chain carbonyl oxygen of Asp[60], and the side chain carboxylate group of this same residue. Relative to the heme in the wild-type MbCO, there is a rotation about the Cβ−Cγ bond of the heme 6-propionate group so that one of its carboxylates moves to within 2.6 Å of the imidazole N_ϵ. Similarly, there is a change in the conformation of the Asp[60] side chain so that its carboxylate group approaches to within 3.0 Å of the His[64] imidazole ring (Figure 3C). This pattern of interactions with three partially or fully negatively charged species implies that the imidazole ring of His[64] is protonated and, moreover, that it may be present as two rapidly exchanging side chain conformers that differ by a 180° $\chi 2$ rotation.

Accompanying the exit of the histidine[64] side chain is the entry of two ordered solvent water molecules into the distal pocket. The first of the water molecules, which is situated 3.1 Å from the oxygen atom of CO, appears to form a hydrogen bond to the main chain carbonyl oxygen of histidine[64], while the second water molecule is located closer to the heme periphery (Figure 3B). It may be significant with regard to the out-of-pocket histidine[64] side chain conformation that the mean Fe−C−O angle in the V68N mutant is 170°, some 10−15° higher than in wild-type MbCO. However, Spiro and co-workers have pointed out that this angle is liable to exhibit large variations with little change in energy (*29*).

Deoxy Forms of Wild-Type and Asn[68] Myoglobin. The deoxy forms of wild-type and V68N myoglobin are very similar to one another with the exception of the position 68 side chain (Figure 4). The iron atoms in the respective structures have retreated ~0.2 Å from the plane of pyrrole nitrogens of the heme toward the proximal side. In contrast to what is observed in sperm whale deoxyMb structures at room temperature, no electron density for distal pocket water is seen in either the A or B molecule of wild-type pig deoxyMb or in the A molecule of V68N deoxyMb at −123 °C. A peak is seen in the heme pocket of the B molecule of the V68N asymmetric unit, and we have placed and refined a water molecule in this density (Figure 4A). The height of this electron density peak is much lower than that associated with the noncoordinated water molecule in the heme pocket of wild-type sperm whale deoxymyoglobin and a number of its mutants which retain the distal histidine in crystals analyzed at room temperature (*10*, *28*). We have also observed clear evidence for a water molecule in the distal pocket of pig V68T deoxymyoglobin at −4 °C (*5*). The absence of a water molecule in the low-temperature structures is probably due to the high osmolarity cryoprotectant and the freezing process itself.

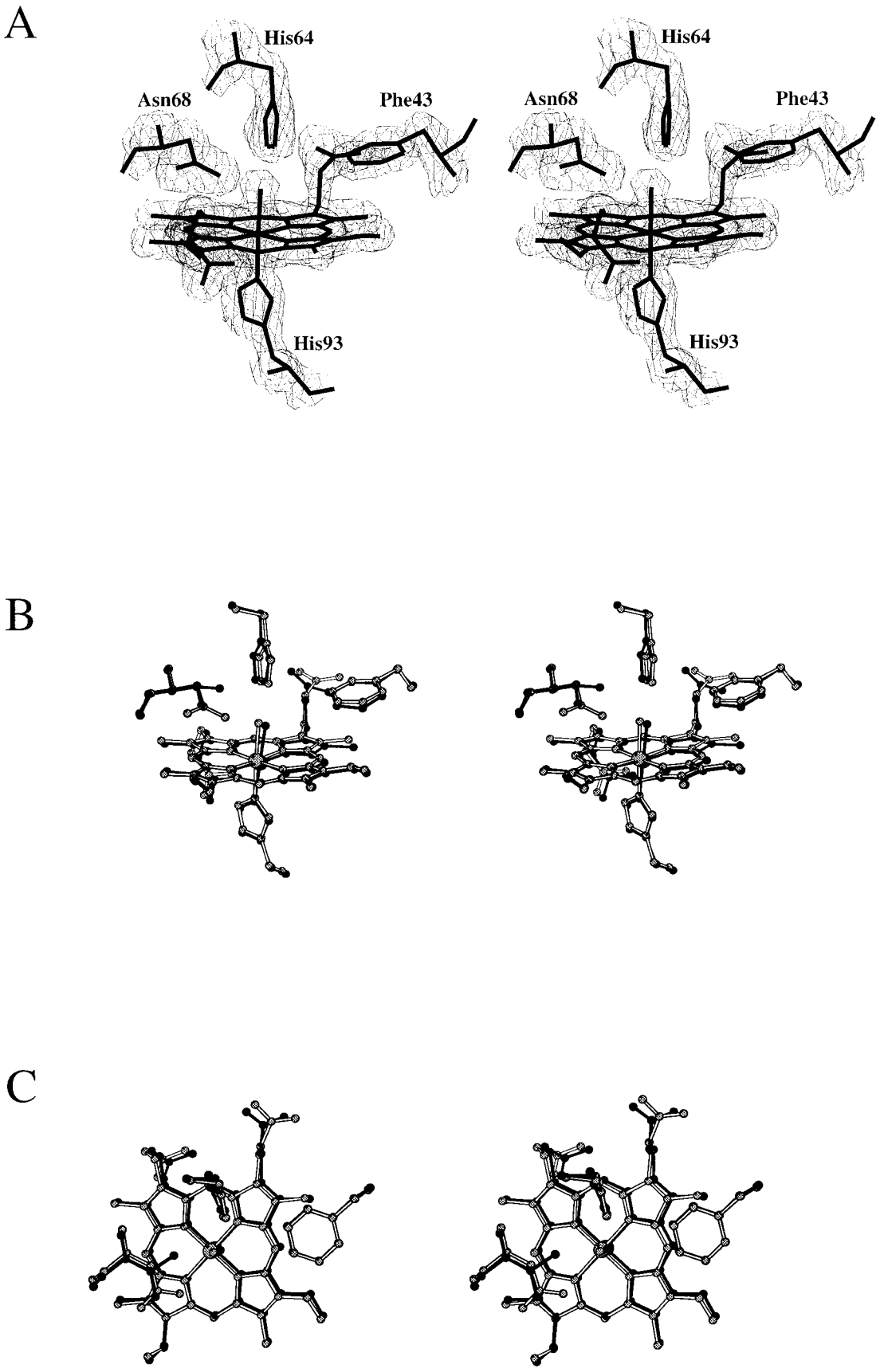

FIGURE 1: (A) $2mF_o - dF_c$, α_{calc} electron density associated with the B molecule of the asymmetric unit of the V68N metmyoglobin crystal. Electron density contoured at the 1.5σ level is shown in the vicinity of the heme pocket with the heme and residues Phe[43] (CD1), His[64] (E7), Asn[68] (E11), and His[93] (F8) shown. (B and C) Orthogonal stereopairs comparing the heme pocket structures of wild-type (dark atoms and bonds) and V68N (shaded atoms and light bonds) myoglobin in the B molecules of the asymmetric unit. The structures were overlaid by least-squares minimization procedures applied to the main chain atoms of residues 5−150.

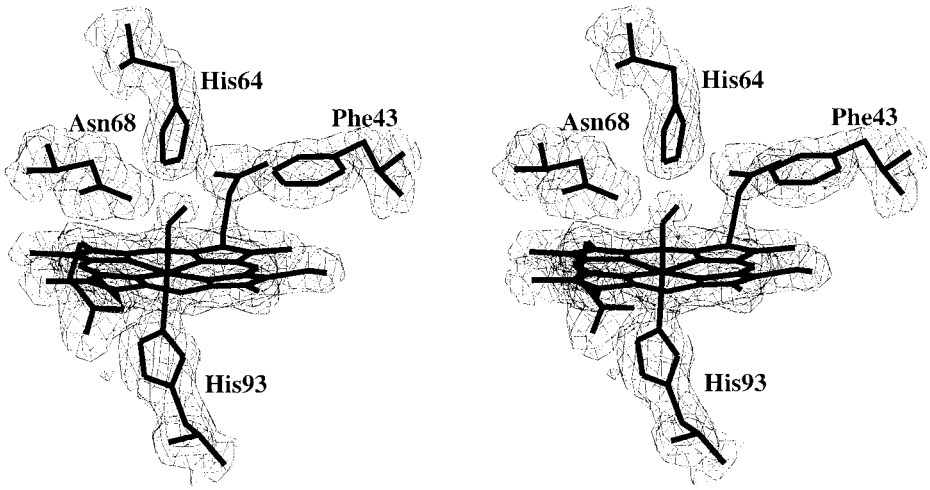

FIGURE 2: Stereoview of the heme pocket and its associated electron density in the B molecule of V68N MbO_2. The map was calculated with coefficients $2mF_o - dF_c$, α_{calc} and is displayed at a contour level 1.5 standard deviations above the average electron density of the map.

Table 2: Heme and Ligand Geometries

	Asn^{68} MbO_2		Asn^{68} MbCO		wild-type MbCO	
	A mol	B mol	A mol	B mol	A mol	B mol
Fe−$N_{pyrrole}$ plane (Å)[a]	0.13	0.13	0.00	0.01	−0.01	−0.01
Fe−Nϵ_2 (F8) (Å)	2.12	2.20	2.07	2.14	2.10	2.10
Fe−O1/Fe−C (Å)	1.81	1.86	1.78	1.82	1.79	1.80
O1−O2/C−O (Å)	1.21	1.23	1.19	1.16	1.22	1.19
∠Fe−O−O/∠Fe−C−O (deg)	134	132	174	174	159	155
NA−Fe−O−O/NA−Fe−C−O (ϕ) (deg)	162	170	168	38	200	213
Nϵ_2 (E7)−OL2 (OL1) (Å)	2.64	2.73	7.61	7.57	3.25	3.28
Nδ_2 (E11)−OL2/Cγ2 (E11)−OL2 (Å)	2.97	2.89	3.29	3.17	3.18	3.22
temperature factors (Å^2)						
Fe	23	22	24	24	22	19
Nϵ_2 (E7)	26	25	33	33	20	21
Nδ_2 (E11)/Cγ_2 (E11)	25	23	21	22	19	19
OL1/C	33	40	22	23	18	19
OL2/O	47	47	26	25	22	21

[a] The displacement of the iron atom from the least-squares plane through the pyrrole nitrogen atoms. A negative value indicates that the iron is displaced to the distal pocket side of the heme.

O_2, CO, and NO Binding. The kinetics of O_2 and CO binding to pig and sperm whale myoglobins was measured by a combination of stopped-flow rapid mixing and laser flash photolysis methods. Rate and equilibrium parameters for wild-type and V68N pig and sperm whale myoglobins are presented in Tables 3 and 4. The overall association rate constant for O_2 is lowered by a factor of 6−9 by the V68N mutation in both mammalian myoglobins. This inhibition could be due to either increased polarity in the distal pocket which further stabilizes noncovalently bound water in the deoxy form or the increased size and rigidity of the E11 side chain which hinders the approach of the ligand to the iron. The O_2 dissociation rate constant is lowered ∼25-fold to 0.6 s^{-1}, consistent with the existence of an "extra" stabilizing hydrogen-bonding interaction between the amide moiety of asparagine[68] and the polar oxygen ligand. This stabilization of bound oxygen implies that the amide $-NH_2$ group is oriented toward the ligand presenting a hydrogen bond donor group to the oxygen. The net result is that the single V68N myoglobin mutants have a 3−4-fold higher affinity for oxygen than the corresponding wild-type proteins.

To test the role of hydrogen bonding, the effects of the V68N substitution were examined in the absence of a distal histidine. As shown in Table 3, Leu[64] sperm whale myoglobin shows a very low oxygen affinity due to an extremely large dissociation rate constant, $k_{O_2} = 4100$ s^{-1}. Insertion of Asn at position 68 in the H64L mutant causes a 160-fold decrease in k_{O_2} giving the H64L/V68N mutant an affinity for oxygen which is significantly greater than that for the wild-type protein. Thus, Asn[68] is clearly able to form a strong hydrogen bond with bound oxygen regardless of the residue present at the 64 (E7) position.

The rate constants for CO binding are also lowered by the V68N replacement. For this ligand the largest effects are on the association rate constants which are decreased 6- and 12-fold in the pig and sperm whale myoglobin mutants, respectively, relative to the wild-type proteins. Boxer and co-workers observed similar effects for CO binding to human V68N Mb (*30*). Since the bimolecular rate constant for CO association with myoglobin has been shown to be limited by the rate of the intramolecular bond formation step, these data imply that there has been a significant decrease in the rate constant for Fe−CO bond formation. The CO dissociation rate constants are ∼2-fold lower in the V68N mutant which may be attributed to a weak but favorable interaction between the positive electrostatic field of the amide $-NH_2$ of asparagine[68] and the $Fe^{\delta+}$=C=$O^{\delta-}$ species (*12*). Similar effects are seen when comparing k_{CO} for H64L

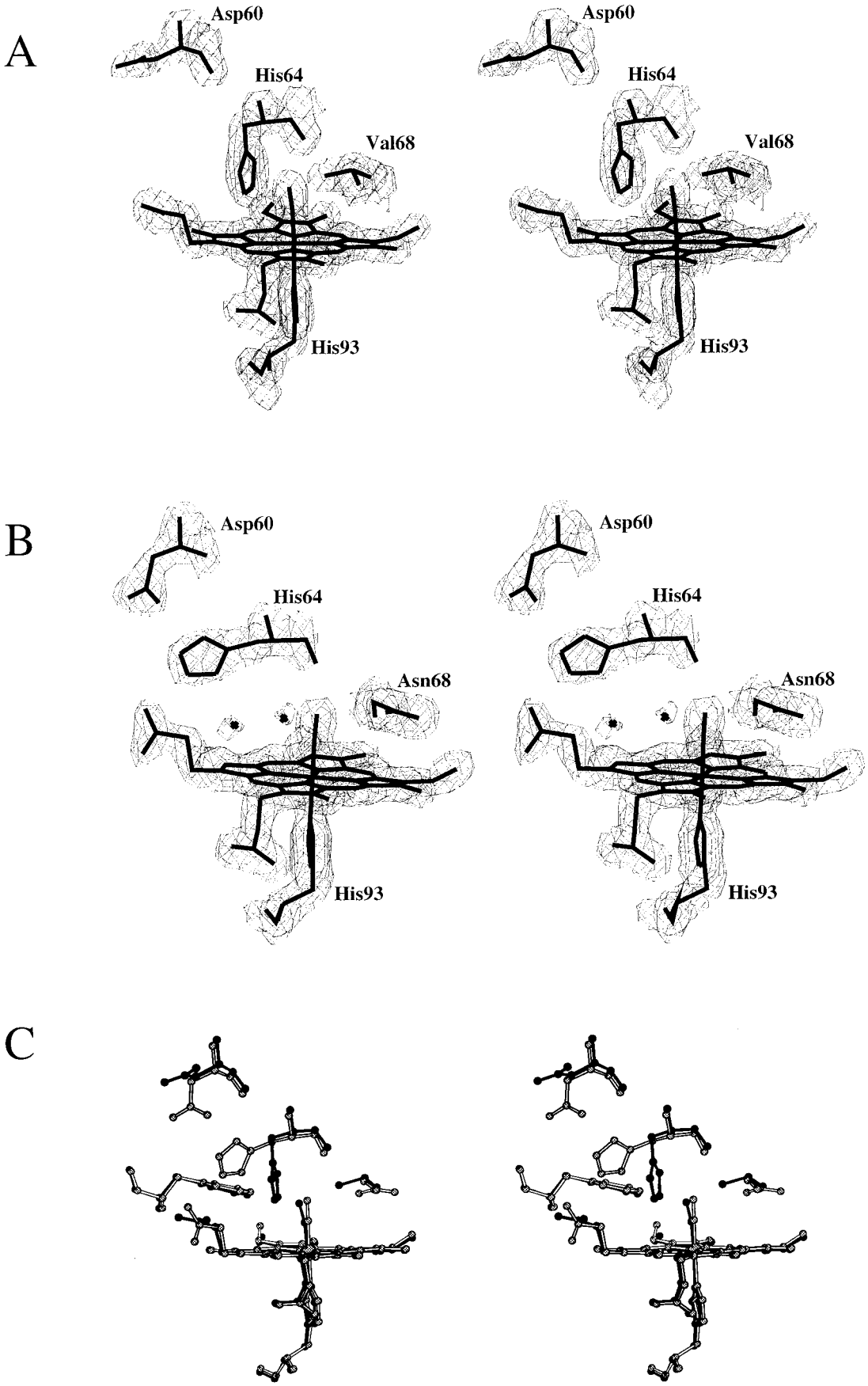

FIGURE 3: Stereoview of the heme environment and associated electron density in the A molecules of the asymmetric unit of (A) wild-type MbCO and (B) V68N MbCO. In each case, the electron density was calculated with coefficients $2mF_o - dF_c$, α_{calc} and displayed at 1.3 standard deviations above the mean value of the map. (C) Structures of wild-type MbCO (dark atoms and bonds) and V68N MbCO (shaded atoms and light bonds) are superimposed after least-squares minimization procedures applied to the main chain atoms of residues 5−150 of the respective A molecules (rmsΔ = 0.23 Å). The altered conformation of the histidine[64] (E7) side chain is apparent.

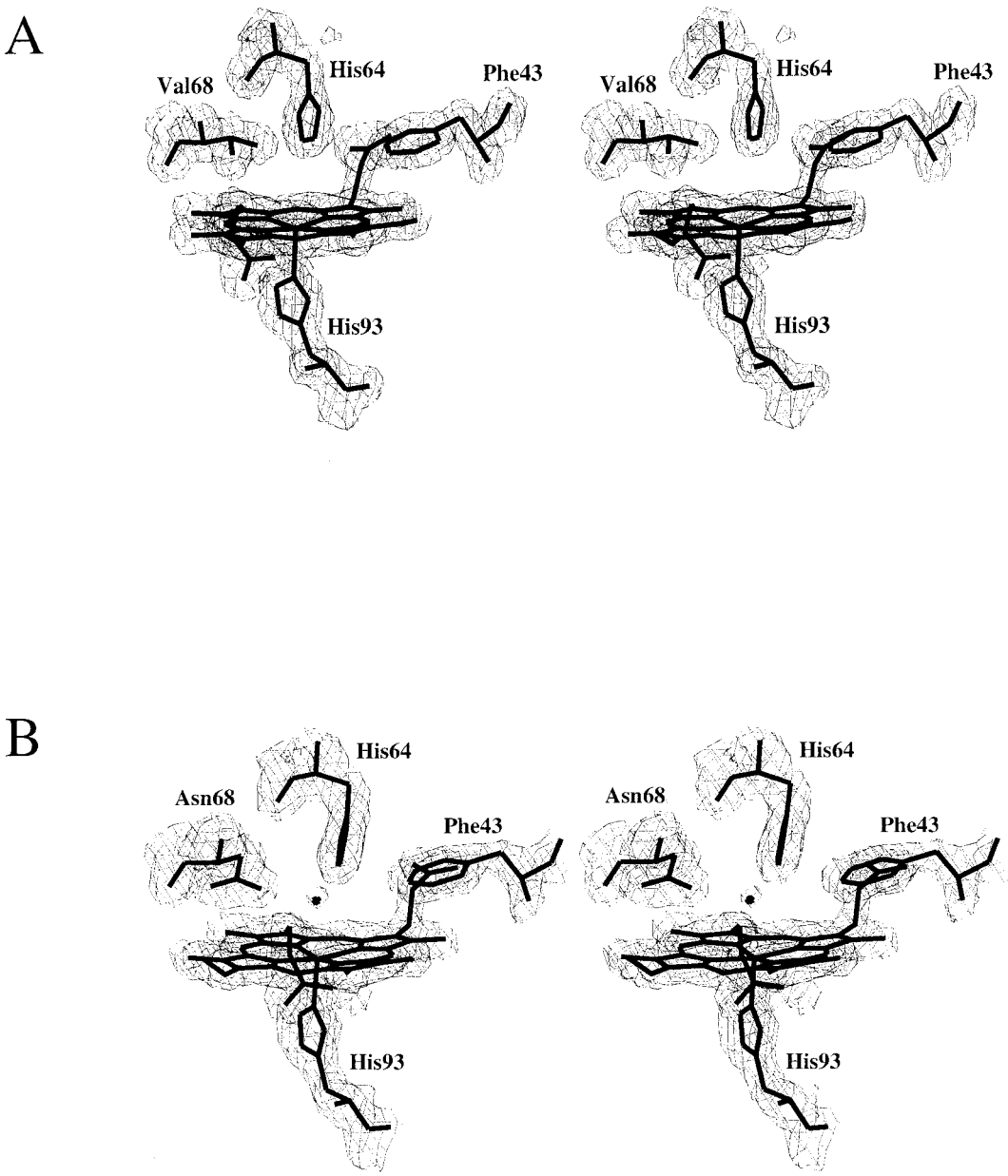

FIGURE 4: Stereoview of the heme pocket structure and associated electron density in the B molecule of (A) wild-type deoxyMb and (B) V68N deoxyMb. The maps were calculated with coefficients $2mF_o - dF_c$ and calculated phases and have been contoured at 1.5 standard deviations above the average electron density of the map. Residues defining the perimeter of the heme pocket are labeled.

Table 3: Kinetic Parameters for O_2 and CO Binding to Wild-Type and V68N Single and Double Mutants of Pig and Sperm Whale Myoglobin

protein	k'_{O_2} (μM^{-1} s^{-1})	k_{O_2} (s^{-1})	K_{O_2} (μM^{-1})	k'_{CO} (μM^{-1} s^{-1})	k_{CO} (s^{-1})	K_{CO} (μM^{-1})	K_{CO}/K_{O_2} (μM^{-1} s^{-1})	k'_{NO} (s^{-1})
wild-type (pig)	17	14	1.2	0.78	0.019	41	34	22
wild-type (SW)	17	15	1.1	0.51	0.019	27	25	27
Asn^{68} (pig)	3.0	0.67	4.5	0.12	0.011	11	2.4	24
Asn^{68} (SW)	1.9	0.54	3.5	0.041	0.0096	4.3	1.2	30
Leu^{64} (SW)	98	4100	0.023	26	0.024	1100	48000	190
$Leu^{64}Asn^{68}$ (SW)	89	40	2.2	15	0.005	3200	1500	nd

and H64L/V68N sperm whale myoglobins. However, introduction of the V68N mutation in the H64L mutant does not cause a significant decrease in either the CO or O_2 association rate constants.

The net result of the single V68N mutation is a 4−6-fold decrease in CO affinity. In contrast, V68N causes a 3-fold increase in K_{CO} in the absence of a distal histidine (H64L/V68N mutant in Table 3). The *M*-values, K_{CO}/K_{O_2}, for the single V68N mutants are close to unity resulting in 15−20-fold more efficient discrimination in favor of oxygen binding than that for the corresponding wild-type myoglobins.

The effects of the V68N mutation on the rate constants for NO association were also examined. As shown in Table

Table 4: Oxygen Rebinding to Wild-Type and Asparagine[68] Mutants of Pig and Sperm Whale Myoglobin[a]

protein	k_{gem} (μs^{-1})	F_{gem}	k'_{entry} (μM^{-1} s^{-1})	k_{escape} (μs^{-1})	k_{bond} (μs^{-1})	k_{-bond} (s^{-1})
wild-type (pig)	32	0.40	42	19	13	23
Asn[68] (pig)	24	0.12	21	21	3	0.8

[a] The observed geminate recombination data were analyzed in terms of the following two-step scheme as described by Quillin et al. (1995):

$$A \text{ or } MbO_2 \underset{k_{escape}}{\overset{k'_{entry}}{\rightleftharpoons}} B, \text{ or ns intermediate} \underset{k_{-bond}}{\overset{k_{bond}}{\rightleftharpoons}} Mb + O_2$$

where $k_{gem} = (k_{bond} + k_{escape})$, $F_{gem} = k_{bond}/(k_{bond} + k_{escape})$, $k'_{O_2} = k'_{entry}F_{gem}$, and $k_{O_2} = k_{-bond}(1 - F_{gem})$.

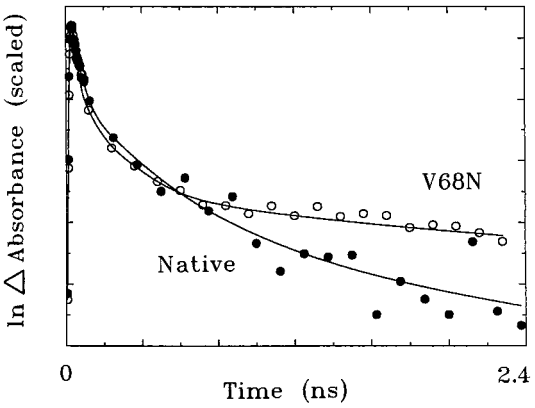

FIGURE 5: Time courses for picosecond geminate recombination of NO in wild-type (native) and V68N pig myoglobin at pH 7.0, 20 °C. The absorbance traces were measured at 436 nm.

3, k'_{NO} is relatively insensitive to the asparagine substitution. This is an interesting observation, because it is known that the overall rate of NO binding to wild-type Mb is governed by the rate of ligand diffusion into the distal heme pocket. The lack of effect of the V68N mutation suggests strongly that the Asn[68] side chain does not significantly stabilize internal water in deoxymyoglobin. The lowered rates of O_2 and CO association must be due to steric hindrance of iron−ligand bond formation which has no effect on k'_{NO}.

Geminate Recombination of NO and O_2. Internal iron−ligand bond formation was examined directly in laser photolysis experiments with both NO and O_2 complexes. Normalized time courses for NO rebinding following a 30-ps laser excitation pulse are shown in Figure 5. The initial picosecond rate of geminate NO rebinding is similar in wild-type and V68N pig myoglobin. However, after about 1 ns the rate of NO rebinding in the mutant protein decreases markedly compared to the wild-type protein with the fraction of unliganded complexes leveling off to roughly 10% of the total that was photolysed.

Molecular dynamics simulations were carried out to interpret the NO rebinding results using the LES method with 10 ligand copies and the program MOIL following the procedures described by Carlson et al. (*31*, *32*). A summary of these computations is presented in Figure 6 which presents the rate of collisions of photodissociated ligands with the iron as a function of the time of the simulation. A collision was defined as occurring when a ligand molecule came within 4 Å of the iron atom. The starting ligand structures were taken from the CO structure of wild-type pig myoglobin and a hypothetical MbNO structure for the V68N mutant.

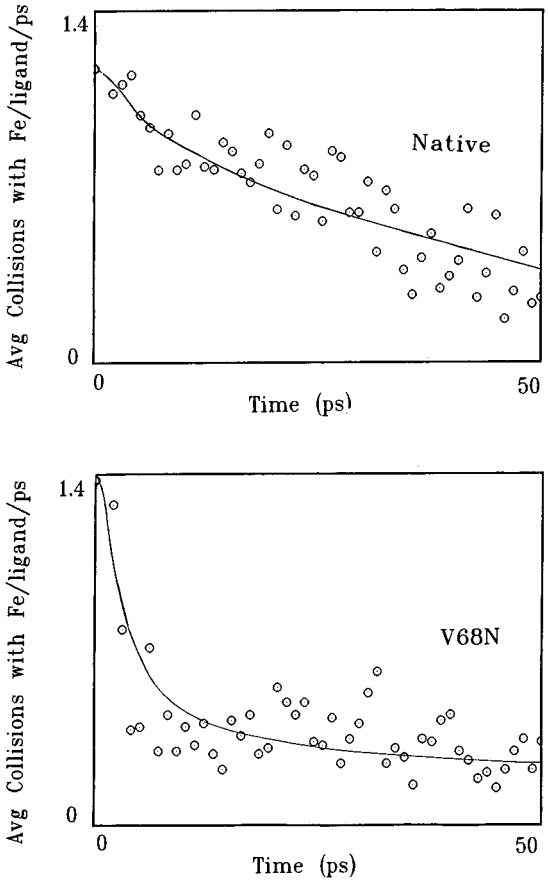

FIGURE 6: Computed rate of collisions of ligands with the iron as a function of the time of molecular dynamic simulation. The *y*-axis values are the number of ligand molecules that come within 4 Å of the iron in 1 ps divided by the number of ligands used in the simulation, usually 10: (A) wild-type (native) Mb and (B) V68N Mb.

The latter structure was nearly identical to the MbO_2 structure for V68N pig myoglobin which was determined after the calculations had been made.

In the simulations for wild-type pig myoglobin, the rate of collisions at the iron atom decreases slowly with time as the ligands progressively move away from the heme center toward the back of the distal pocket (Figure 6A). The ligand trajectories are almost identical to those seen for wild-type sperm whale myoglobin which have been described in detail (*32*). In contrast, the rate of collisions at the iron atom in the V68N mutant decreases rapidly in the first few picoseconds of the simulation and then levels off to very small value near 0 (Figure 6B). In the mutant protein the ligands quickly move away from the iron atom toward Ile[107] and then are blocked from reapproaching it by the planar amide group of the large asparagine[68] side chain. This phenomenon appears to be the underlying cause for the slow rate of ligand recombination on the longer nanosecond time scales for all ligands.

Figure 7 shows time courses for the geminate recombination of O_2 with wild-type and V68N pig myoglobin following photolysis with a 9-ns laser pulse. As expected from the NO results, the fraction of the photolysed O_2 which recombines on the nanosecond time scale is much smaller for the V68N mutant. Table 4 presents the geminate rate parameters evaluated in terms of a two-step rebinding scheme

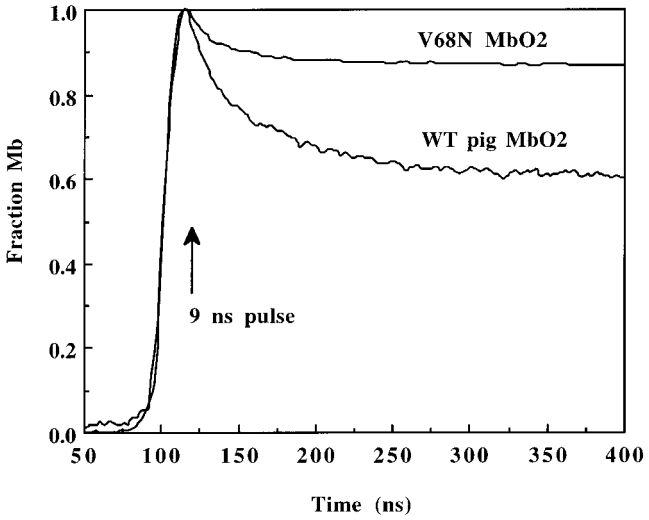

FIGURE 7: Rebinding of O_2 to wild-type and V68N pig oxymyoglobin following a 9-ns excitation pulse. The reactions were carried out at 20 °C, pH 7.0, and absorbance traces were measured at 436 nm.

(i.e., MbX or A ↔ B ↔ Mb + X, where B is the nanosecond geminate intermediate) (*33*). The fitted first-order geminate rate constants are about the same for the mutant and wild-type pig proteins. Thus, the decrease in the fraction of geminate rebinding for the mutant must be due to a decrease in the rate of iron−ligand bond formation (k_{bond} in Table 4), as suggested by the simulations for NO rebinding shown in Figure 6. In contrast, the rate of ligand escape from pig myoglobin remains unaffected by the V68N substitution.

Table 4 shows that the largest effect of the V68N mutation is on the rate constant associated with breaking of the Fe−O−O bond (k_{-bond}). This rate of thermal bond disruption is decreased by a factor of 30, presumably due to additional hydrogen bonding to the $-NH_2$ of the asparagine^{68} side chain. Since the rate constant for rebinding of O_2 from within the pocket is also lowered by a factor of 4, the net effect of the mutation is a 7-fold increase in the equilibrium constant for O_2 binding from within the distal heme pocket (k_{bond}/k_{-bond}). As predicted from the overall rate constants for NO association, the V68N mutation has little effect on the rate of ligand movement into heme pocket (k'_{entry}). The apparent equilibrium constant for noncovalent association ($K_{entry} = k'_{entry}/k_{entry}$) is only a factor of 2 lower than that for the wild-type protein.

Building on the work of Chatfield et al. (*34*), Scott and Gibson (*35*) have reexamined geminate O_2 rebinding to sperm whale myoglobin mutants on time scales ranging from 9 to 4000 ns. Detailed analyses of the time courses revealed two phases. The slow phase comprised about 25% of the total extent of recombination and was shown to be due to ligand migration into and back from secondary sites or cavities in the interior of the protein. Similar phenomena appear to occur for all mammalian myoglobins including the pig protein if recombination is examined on long time scales. However, the V68N single mutant shows little evidence for a secondary phase, presumably because rebinding from both the primary and secondary sites is inhibited significantly by the Asn side chain. As a result, we have compared the wild-type and mutant results using the simpler but approximate two-step scheme described in Table 4.

DISCUSSION

Site-directed mutagenesis studies of myoglobin have emphasized the contribution of the distal histidine residue in discriminating between oxygen and carbon monoxide ligands. This side chain forms a strong hydrogen bond with the highly polar Fe−O_2 complex, an electrostatic interaction which stabilizes the bound dioxygen by a factor of ∼1000 relative to simple model heme compounds or mutants with an apolar residue at the E7 position (*2*). This contribution is offset in part however, because His^{64} (E7) draws a water molecule into the distal pocket of deoxymyoglobin, and the requirement for displacement of this water inhibits ligand binding by a factor of ∼10. As a result, K_{O_2} for myoglobin is only a factor of 100 higher than in the apolar E7 mutants. In the case of carbon monoxide, the electrostatic interaction with histidine^{64} is much weaker and the ligand is stabilized by a factor of only 3. This does not offset the stabilization conferred on the water in deoxyMb, and as a result K_{CO} is actually diminished 3-fold by the presence of the distal histidine.

Replacement of the apolar valine at position E11 with asparagine causes effects on ligand-binding equilibria which support the electrostatic stabilization theory. Oxygen bound to either pig or sperm whale V68N myoglobin is stabilized 30-fold relative to wild-type myoglobin based on comparisons of both the overall k_{O_2} and the rate of thermal bond disruption computed from geminate recombination data. This favorable influence is offset by enhanced steric hindrance of iron−ligand bond formation due to the larger size and planarity of the amide side chain. The net result is a modest 4-fold increase in K_{O_2}. Similar considerations explain the 5-fold decrease in K_{CO}. A modest but favorable electrostatic interaction occurs between the asparagine amide and the FeCO, but this is more than offset by the enhanced steric hindrance. The key role of favorable hydrogen bonding is again seen in the results for the H64L/V68N double mutant. In this case, the V68N mutation causes a 160-fold enhancement of O_2 affinity in the presence of leucine at position 64 (E7). The 30−160-fold stabilization of bound oxygen by Asn^{68} relative to the 1000-fold stabilization conferred by His^{64} in the wild-type protein is readily explained by differences in the hydrogen bond distances and geometries revealed in the crystal structures. The $-N_\delta$ of Asn^{68} is situated ∼0.2 Å further from the ligand than the N_ϵ of His^{64}; whereas the latter is close to and can interact with both O1 and O2 of the ligand, the former is close only to O2 (Table 2).

The geminate recombination data for O_2 rebinding to pig myoglobin show that the V68N mutation causes only a 2-fold lowering of the rate constant for ligand movement from the solvent into the protein (k'_{entry} in Table 4). This result suggests that the water molecule in V68N deoxymyoglobin is not significantly stabilized by the asparagine substitution, in marked contrast to the observations with the V68T substitution where ligand partitioning into the heme pocket was reduced 25-fold. Presumably, any favorable polar interactions between the distal pocket water and Asn^{68} are offset by steric hindrance due to the larger size of the amide side chain. The crystal structures of the low-temperature deoxy forms of wild-type and V68N myoglobin neither support nor contradict this conclusion since neither contain

well-defined distal pocket water molecules. These low-temperature results are in contrast to the room-temperature structures of wild-type and a number of mutant deoxymyoglobins where distal pocket water molecules are well-defined (*10*, *28*). We assume their absence here is caused by the high osmolarity of the solutions used as cryoprotectant.

The effects of the valine[68] to asparagine mutation on the ligand association rate constants resemble those for the valine[68] to isoleucine substitution in sperm whale myoglobin. This mutation also lowers k'_{O_2} and k'_{CO} without changing k'_{NO}. Furthermore, the geminate rebinding kinetic traces for V68I and V68N are very similar (*10*). The crystal structure of the deoxy form of V68I shows that the *sec*-butyl side chain of isoleucine[68] resides over the iron and sterically hinders ligand binding such that in the crystal structure of the MbCO form this side chain significantly populates an alternate, and less sterically hindering, conformation. In the V68L Mb, the isobutyl side chain also adopts two or more conformations upon CO ligation in the crystal, implying that the leucine side chain again hinders ligand binding. However, the extent of this hindrance must be small since the rate constants for ligand association in this mutant are similar to or larger than those of the wild-type protein (*10*). In the case of V68N, the barriers to reorientation of the planar amide group of the asparagine[68] side chain are likely to be greater than those for leucine[68], so that as for V68I, the effects of steric hindrance are manifested in the overall and geminate rebinding kinetics.

The upward movement of the distal histidine in the crystal structure of V68N MbCO was somewhat unexpected, although similar displacements of this side chain have been observed previously in wild-type myoglobin. In the presence of bulky ligands such us alkyl isocyanides, phenylhydrazine, and imidazole, the histidine side chain significantly populates an out-of-pocket conformation (*36*−*39*). In MbCO complexes at pH 4, the electron density associated with the histidine E7 indicates two conformations with the distal histidine swinging in and out of the heme pocket (*40*). A similar outward conformation is seen in the aquomet and CO structures of F46V sperm whale myoglobin in which the "hole" created at the CD4 position allows greater freedom of movement of the distal histidine side chain (*41*).

In the present study of a low-temperature MbCO mutant crystal, the electron density describes the out-of-pocket conformation of the distal histidine unambiguously. There are at least three possible causes for this movement. First, the Asn[68] may neutralize any favorable electrostatic interactions between bound CO and His[64], allowing greater flexibility of the imidazole side chain. Second, the extra bulk of the asparagine and its inflexible planar amide group may inhibit inward bending of the Fe−CO complex which would in turn "push" His[64] toward the solvent interface. Third, the enhanced polarity of the distal pocket may raise the pK_a of the distal histidine facilitating its protonation and solvation.

The upward movement of the histidine in V68N MbCO helps to explain the complex infrared absorbance spectrum of this mutant which includes components at 1916 (∼60%) and 1940 cm^{-1} and a broad weak band at 1960 cm^{-1} (*11*, *12*, *42*). Li et al. (*12*) have shown that the IR stretching frequency of CO in Mb is a sensitive gauge of the electrostatic potential around the ligand; positive charges from proton donors decrease the CO bond order and the stretching frequency, while negative charges have the opposite effect. For example, replacement of the distal histidine with an apolar residue causes the principal CO stretching frequency to rise from 1945 to 1966 cm^{-1}. The multiple CO conformations implied by the spectrum of V68N MbCO can be interpreted as follows. (1) The 1916-cm^{-1} band is the result of interactions of bound CO with both the $-NH_2$ of Asn[68] and either the $-N_\epsilon H$ of His[64] or the positive component of the dipole of a water molecule. (2) The 1940-cm^{-1} band is due to interaction with only the NH_2 of Asn[68]. (3) The weak 1960-cm^{-1} band is due to interaction with the carbonyl O atom of the Asn[68] amide side chain and/or the partial negative charge of the water molecule which replaces the distal histidine at the protein−solvent interface (Figure 4).

In view of its ability to stabilize bound O_2 and enhance discrimination against CO, why does Asn[68] (E11) not occur in nature? The principal cause of selection against Asn[68] in nature appears to be its inhibitory effect on apoglobin stability. The biosynthesis of myoglobin inside cells requires that the newly synthesized polypeptide chain fold up to form the native myoglobin tertiary structure. The apomyoglobin then captures ferric heme to form metmyoglobin which is subsequently reduced to the ferrous species. In a comprehensive survey of myoglobin mutants, Hargrove et al. (*13*) showed that polar substitutions in the distal heme pocket greatly destabilize apomyoglobin. The yields of recombinant mutant myoglobins in which polar substitutions have been introduced into the heme pocket are very low presumably because the polypeptide is degraded intracellularly before it is able to fold and take up heme. This problem is circumvented when these mutants are expressed as inclusion bodies. The protein can then be solubilized and refolded by in vitro addition of heme in the absence of predatory proteases. Replacement of the distal histidine with apolar side chains also stabilizes apomyoglobin markedly. However, in this case, histidine[64] is an absolute requirement for the physiological necessities of (1) higher oxygen affinity, (2) efficient discrimination against CO binding, and (3) resistance to autoxidation (*43*). A compromise between function and stability has therefore been reached.

REFERENCES

1. Springer, B. A., Sligar, S. G., Olson, J. S., and Phillips, G. N., Jr. (1994) *Chem. Rev. 94*, 699−714.
2. Olson, J. S., and Phillips, G. N., Jr. (1997) *J. Biol. Inorg. Chem. 2*, 544−552.
3. Springer, B. A., Egeberg, K. D., Sligar, S. G., Rohlfs, R. J., Mathews, A. J., and Olson, J. S. (1989) *J. Biol. Chem. 264*, 3057−3060.
4. Smerdon, S. J., Dodson, G. G., Wilkinson, A. J., Gibson, Q. H., Blackmore, R. S., Carver, T. E., and Olson, J. S. (1991) *Biochemistry 30*, 6252−6260.
5. Cameron, A. D., Smerdon, S. J., Wilkinson, A. J., Habash, J., Helliwell, J. R., Li, T., and Olson, J. S. (1993) *Biochemistry 32*, 13061−13070.
6. Carver, T. E., Brantley, R. E., Jr., Singleton, E. W., Arduini, R. M., Quillin, M. L., Phillips, G. N., Jr., Olson, J. S., and Gibson, Q. H. (1992) *J. Biol. Chem. 267*, 14443−14450.
7. Kloek, A. P., Yang, J., Mathews, F. S., Frieden, C., and Goldberg, D. E. (1994) *J. Biol. Chem. 269*, 2377−2379.
8. Gibson, Q. H., Regan, R., Olson, J. S., Carver, T. E., Dixon, B., Pohajdak, B., Sharma, P. K., and Vinogradov, S. N. (1993) *J. Biol. Chem. 268*, 16993−16998.

9. Travaglini Allocatelli, C., Cutruzzola, F., Brancaccio, A., Vallone, B., and Brunori, M. (1994). *FEBS Lett. 352*, 63−66.
10. Quillin, M. L., Li, T., Olson, J. S., Phillips, G. N., Jr., Dou, Y., Ikeda-Saito, M., Regan, R., Carlson, M., Gibson, Q. H., Li, H., and Elber, R. (1995) *J. Mol. Biol. 245*, 416−436.
11. Balasubramanian, S., Lambright, D. G., and Boxer, S. G. (1993) *Proc. Natl. Acad. Sci. U.S.A. 90*, 4718−4722.
12. Li, T., Quillin, M. L., Phillips, G. N., Jr., and Olson, J. S. (1994) *Biochemistry 33*, 1433−1446.
13. Hargrove, M. S., Krzywda, S., Wilkinson, A. J., Dou, Y., Ikeda-Saito, M., and Olson, J. S. (1994) *Biochemistry 33*, 11767−11775.
14. Hargrove, M. S., Wilkinson, A. J., and Olson, J. S. (1996) *Biochemistry 35*, 11300−11309.
15. Lehmann, H. (1986) in *Hemoglobin: Molecular, Genetic and Clinical Aspects* (Bunn, H. F., and Forget, B. G., Eds.) W. B. Saunders Co., Philadelphia, PA.
16. Nagai, K., and Thørgeren, H.-C. (1984) *Nature 309*, 810−812.
17. Carver, T. E., Olson, J. S., Smerdon, S. J., Krzywda, S., Wilkinson, A. J., Gibson, Q. H., Blackmore, R. S., Dezz Ropp, J., and Sligar, S. G. (1991) *Biochemistry 30*, 4697−4705.
18. Dodson, G. G., Hubbard, R. E., Oldfield, T. J., Smerdon, S. J., and Wilkinson, A. J. (1988) *Protein Eng. 2*, 233−237.
19. Otwinowski, Z., and Minor, W. (1997) *Methods Enzymol. 276*, 307−326.
20. CCP4, Collaborative Computational Project, No. 4. (1994) The CCP4 suite: programs for protein crystallography. *Acta Crystallogr. D50*, 760−763.
21. Murshudov, G. N., Vagin, A. A., and Dodson, E. J. (1997) *Acta Crystallogr. D53*, 240−255.
22. Oldfield, T. J. (1996) in *Macromolecular Refinement. Proceedings of the CCP4 Study Weekend* (Dodson, E. J., Moore, M. H., Ralph, A., and Baily, S., Eds.) pp 67−74, SERC Daresbury Laboratory, Warrington, U.K.
23. Murshudov, G. N., Davies, G. J., Isupov, M., Krzywda, S., and Dodson, E. J. (1998) in *CCP4 Newsletter on Protein Crystallography* (Bailey, S., and Winn, M., Eds.) pp 37−42, CLRC Daresbury Laboratory, Warrington, U.K.
24. Rohlfs, R. J., Mathews, A. J., Carver, T. E., Olson, J. S., Springer, B. A., Egeberg, K. D., and Sligar, S. G. (1990) *J. Biol. Chem. 265*, 3168−3176.
25. Carver, T. E., Rohlfs, R. J., Olson, J. S., Gibson, Q. H., Blackmore, R. S., Springer, B. A., and Sligar, S. G. (1990) *J. Biol. Chem.* 265, 20007−20020.
26. Gibson, Q. H., Regan, R., Elber, R., Olson, J. S., and Carver, T. E. (1992) *J. Biol. Chem. 267*, 22022−22034.
27. Oldfield, T. J., Smerdon, S. J., Dauter, Z., Petratos, K., Wilson, K. S., and Wilkinson, A. J. (1992) *Biochemistry 31*, 8732−8739.
28. Quillin, M. L., Arduini, R. M., Olson, J. S., and Phillips, G. N., Jr. (1993) *J. Mol. Biol. 234*, 140−155.
29. Spiro, T. G., and Kozlowski, P. M. (1997) *J. Biol. Inorg. Chem. 2*, 516−520.
30. Balasubramanian, S., Lambright, D. G., Marden, M. C., and Boxer, S. G. (1993) *Biochemistry 32*, 2202−2212.
31. Carlson, M. L., Regan, R., Elber, R., Li, H. Y., Phillips, G. N., Olson, J. S., and Gibson, Q. H. (1994) *Biochemistry 33*, 10597−10606.
32. Carlson, M. L., Regan, R., and Gibson, Q. H. (1996) *Biochemistry 35*, 1125−1136.
33. Olson, J. S., and Phillips, G. N., Jr. (1996) *J. Biol. Chem. 271*, 17593−17596.
34. Chatfield, M. D., Walda, K. N., and Magde, D. (1990) *J. Am. Chem. Soc. 112*, 4680−4687.
35. Scott, E. E., and Gibson, Q. H. (1997) *Biochemistry 36*, 11909−11917.
36. Johnson, K. A., Olson, J. S., and Phillips, G. N., Jr. (1989) *J. Mol. Biol. 207*, 459−463.
37. Ringe, D., Petsko, G. A., Kerr, D. E., and Ortiz de Montellano, P. R. (1984) *Biochemistry 23*, 2−4.
38. Bolognesi, M., Cannillo, E., Ascenzi, P., Giacometti, G. M., Merli, A., and Brunori, M. (1982) *J. Mol. Biol. 158*, 305−315.
39. Johnson, K. A. (1993) Ph.D. Dissertation, Rice University.
40. Yang, F., and Phillips, G. N., Jr. (1996) *J. Mol. Biol. 256*, 762−774.
41. Lai, H. H., Li, T. S., Lyons, D. S., Phillips, G. N., Jr., Olson, J. S., and Gibson, Q. H. (1995) *Proteins Struct. Funct. Genet. 22*, 322−329.
42. Anderton, C. L., Hester, R. E., and Moore, J. N. (1997) *Biochim. Biophys. Acta 1338*, 107−120.
43. Brantley, R. E., Smerdon, S. J., Wilkinson, A. J., Singleton, E. W., and Olson, J. S. (1993*) J. Biol. Chem. 268*, 6995−7010.

BI9812470